Journal of Applied Physics ARTICLE scitation.org/journal/jap

Nanoscale X-ray imaging of spin dynamics in yttrium iron garnet

Cite as: J. Appl. Phys. **126**, 173909 (2019); doi: 10.1063/1.5121013
Submitted: 22 July 2019 · Accepted: 17 October 2019 ·
Published Online: 5 November 2019

J. Förster,[1,a)] S. Wintz,[2,3] J. Bailey,[2,4] S. Finizio,[2] E. Josten,[3,5] C. Dubs,[6] D. A. Bozhko,[7,8,9] H. Stoll,[1,10] G. Dieterle,[1] N. Träger,[1] J. Raabe,[2] A. N. Slavin,[11] M. Weigand,[1,12] J. Gräfe,[1] and G. Schütz[1]

AFFILIATIONS

[1]Max-Planck-Institut für Intelligente Systeme, 70569 Stuttgart, Germany
[2]Paul Scherrer Institut, 5232 Villigen, PSI Switzerland
[3]Helmholtz-Zentrum Dresden-Rossendorf, 01328 Dresden, Germany
[4]École polytechnique fédérale de Lausanne (EPFL), 1015 Lausanne, Switzerland
[5]Ernst Ruska-Centre for Microscopy and Spectroscopy with Electrons (ER-C) and Peter Grünberg Institute (PGI), Forschungszentrum Jülich, 52425 Jülich, Germany
[6]INNOVENT e.V. Technologieentwicklung Jena, 07745 Jena, Germany
[7]Fachbereich Physik, Technische Universität Kaiserslautern, 67663 Kaiserslautern, Germany
[8]Departement of Physics, University of Colorado at Colorado Springs, Colorado Springs, Colorado 80918, USA
[9]University of Glasgow, G12 8LT Glasgow, United Kingdom
[10]Institut für Physik, Johannes Gutenberg-Universität Mainz, 55122 Mainz, Germany
[11]Department of Physics, Oakland University, MI-48309 Rochester, Michigan, USA
[12]Helmholtz-Zentrum Berlin, 14109 Berlin, Germany

[a)]jfoerster@is.mpg.de

ABSTRACT

Time-resolved scanning transmission x-ray microscopy has been used for the direct imaging of spin-wave dynamics in a thin film yttrium iron garnet (YIG) with sub-200 nm spatial resolution. Application of this x-ray transmission technique to single-crystalline garnet films was achieved by extracting a lamella ($13 \times 5 \times 0.185\,\mu\text{m}^3$) of the liquid phase epitaxy grown YIG thin film out of a gadolinium gallium garnet substrate. Spin waves in the sample were measured along the Damon-Eshbach and backward volume directions of propagation at gigahertz frequencies and with wavelengths in a range between 200 nm and 10 μm. The results were compared to theoretical models. Here, the widely used approximate dispersion equation for dipole-exchange spin waves proved to be insufficient for describing the observed Damon-Eshbach type modes. For achieving an accurate description, we made use of the full analytical theory taking mode-hybridization effects into account.

I. INTRODUCTION

Spin waves are collective magnetic excitations in ferro-, ferri-, and antiferromagnetic materials and an active research area in the field of magnetism. Recently, it was demonstrated that their quanta, magnons, show specific fundamentals of bosonic behavior such as Bose-Einstein condensation and superfluidity.[1,2] Also, even black hole scenarios have been predicted to occur in magnon gases.[3] Besides the fundamental impact of this topic, there has also been increasing interest in potential applications of spin waves as information carriers. This has led to the emergence of the field of magnonics. Compared to electromagnetic waves, spin-wave wavelengths are smaller by several orders of magnitude, which fits perfectly to the lateral dimensions of $10\,\text{nm} - 1\,\mu\text{m}$ achievable by modern nanotechnology. Spin waves excellently cover the Gigahertz-regime of frequencies, which is common in today's communications devices, allowing their creation and detection via well-developed microwave techniques. Furthermore, and in contrast to conventional electronics, spin waves can carry information without power dissipating charge currents. Therefore, spin waves are actively discussed as high-speed and short-wavelength information carriers for novel spintronic/magnonic devices,[4,5] in particular with respect to quantum effects and computing at low temperatures.[6,7]

Magnetic thin film systems exhibit three basic geometries for lateral spin wave propagation in their spectrum (cf. Fig. 1). For in-plane magnetized films, there is the backward volume (BV) geometry with waves propagating along the equilibrium magnetization direction, as well as the Damon-Eshbach (DE) geometry, in which the waves propagate perpendicular to it. Forward volume waves occur in films magnetized out-of-plane propagating isotropically in any direction in the film plane.[4,8–11] Finally, in addition to the fundamental modes with a quasiuniform amplitude profile over the film thickness, all three geometries possess higher order thickness modes with amplitude profiles in the form of perpendicular standing spin waves (PSSW) between the two film surfaces.[12] The relevant energy contributions that determine the dispersion relations $f(k = 2\pi/\lambda)$ of the spin waves in these geometries are the magnetostatic and exchange interactions, which dictate the long- and short-wavelength regimes, respectively.[12]

The insulating ferrimagnet yttrium iron garnet (YIG) is one of the most prominent and extensively studied materials in the field of magnonics due to its exceptionally low magnetic damping and

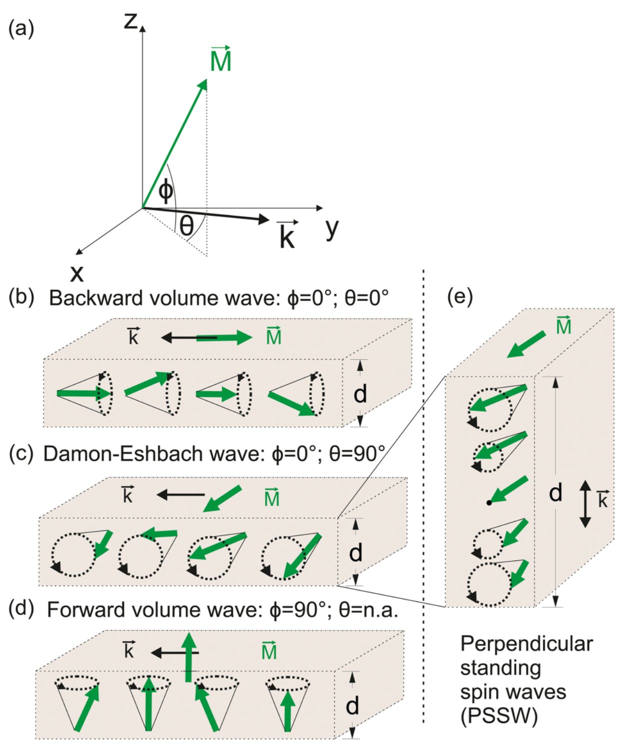

FIG. 1. Overview of the basic spin-wave mode geometries in a magnetic thin film of thickness *d*. Green arrows symbolize the magnetization vector **M**, while the black ones show the wave vector **k**.

high spin-wave propagation length, making it ideal as a model system[13–15] and for possible applications.[4,9,16–18] Studies become sparse, however, for wavelengths and spatial features below 250 nm, despite the importance of this regime for potential nanoscale spintronic devices and the open questions it holds. Factors such as surface effects, crystal defects, grain sizes or spin diffusion become more influential on this scale[19,20] and can change spin-wave behavior compared to the well-studied microscale. For example, an increase in spin wave damping as well as the emergence of frequency dependent damping[19,20] are expected at the nanoscale. The main reason for this region being less well studied lies in its experimental accessibility. The direct imaging of spin-wave dynamics is conventionally performed by optical techniques like Kerr microscopy[21,22] and Brillouin light scattering,[4,5,23] which are typically limited to a spatial resolution of about 250 nm and the scattering of corresponding optical wavelengths,[24,25] respectively. Therefore, optical methods are unable to access nanoscale waves and devices—with the partial exception of a near-field approach.[26,27] Another commonly used experimental technique for studying spin waves is all electrical spin-wave spectroscopy using vector network analyzers.[28,29] While this method is not directly limited by the wavelength, it does not allow for a direct imaging of spin waves. It also needs comparably large samples to achieve sufficient signal to noise ratio,[30] limiting its access to nanoscale devices. Thus, from both a fundamental and applications perspective, there is a clear need for the spatially resolved detection of sub-250 nm spin waves.

Time-resolved scanning transmission x-ray microscopy (TR-STXM) is a technique that is able to meet these requirements.[31–42] Magnetic phenomena can be routinely studied with spatial and stroboscopic temporal resolutions down to 20 nm and 50 ps, respectively. Spin waves in metallic samples prepared as thin films on x-ray transparent silicon nitride (SiN) membranes have already been imaged successfully.[43–47] But the lack of x-ray transparency in the bulk substrates of single-crystalline systems like YIG films on gadolinium gallium garnet (GGG) requires an appropriate thinning route for STXM investigations.[48,49] Therefore, in the present work, a thin sheet of YIG of 185 nm thickness has been sliced out of a YIG thin film and its GGG substrate. The lamella was subsequently put onto an x-ray transparent SiN membrane (cf. Sec. II). We present TR-STXM measurements in YIG, which provide a new view on the rich and complex scenario of the spin-wave characteristics, their interactions, and coexistence in the nanometer range of this pivotal model system for design and understanding of future magnonic/spintronic applications.

II. METHODS

A YIG film of (185 ± 1) nm thickness, as measured by a prism coupler, was grown by liquid phase epitaxy (LPE) on the (111)-oriented GGG.[50] Ferromagnetic resonance measurements showed a saturation magnetization of $M_S = (143 \pm 2)$ kA/m and a Gilbert damping coefficient of $\alpha = 3 \times 10^{-5}$ at an inhomogeneous line broadening of $\mu_0 \Delta H_0 = 0.13$ mT, which agree well with typical values for YIG films in the literature.[4,50–52] The particular YIG film thickness of 185 nm was chosen in order to allow for a sufficient soft x-ray transmission on the one hand side, while sustaining a Gilbert damping value close that of corresponding bulk systems on the other hand. The film was further processed using a "FEI Dual Beam System Helios NanoLab 460F1" focused ion beam (FIB). A dedicated Ga^+ ion milling routine[53] resulted in a lamella of $13 \times 5 \times 0.185\,\mu m^3$ of YIG with less than 150 nm GGG attached to it. Afterward, an "Omniprobe" micromanipulator was used to transfer the lamella to a standard SiN membrane, where it was centered on a copper microstrip antenna ($2\,\mu$m width and 200 nm thickness) and fixated with carbon. The copper microstrip was fabricated prior to the fixation of the lamella by a combination of electron beam lithography, thermal copper evaporation, and lift-off processing.

Measurements have been carried out at the MAXYMUS end station located at the UE46-PGM2 beam line at the BESSY II synchrotron radiation facility of Helmholtz-Zentrum Berlin. Circularly polarized x-rays were focused to 20 nm by a Fresnel zone plate. The X-ray magnetic circular dichroism (XMCD) effect[54] was used as the magnetic contrast mechanism for imaging. For the x-ray energy, the iron L_3-absorption edge was chosen, where the maximum magnetic signal fidelity was found at (708 ± 0.3) eV as a balance between the XMCD strength and the transmitted intensity.[55] The sample was mounted in the normal incidence geometry, sensitive to the out-of-plane magnetization component. A quadrupole permanent magnet system provided an in-plane magnetic bias field in the range of ± 250 mT.[37] Spin waves were excited by the magnetic field of an RF-current flowing through the copper strip line (cf. Fig. 2).

Time-resolution has been achieved by using a stroboscopic pump-and-probe technique that reaches a resolution of around 50 ps during the synchrotron's regular multibunch mode operation.[38] The raw movies from TR-STXM were normalized to enhance the dynamics. A pixel-wise fast Fourier transform (FFT) in the time domain was subsequently used to obtain the local spin-wave amplitude and phase,[56,57] which were then used to visualize the waves in HSV (hue, saturation, value) color space (cf. Fig. 2). A two-dimensional FFT in space was utilized to determine the corresponding wave vectors. See also the paper of Groß *et al.*[47] for more details on this.

III. RESULTS

A. Experimental results

As a first step, a continuous RF-current in the frequency range of 1.4 to 3.0 GHz was used for excitation. Figure 2(a) shows the sample architecture and images of dynamics measured at different frequencies with an external magnetic field of $\mu_0 H_{ext} = 25$ mT applied parallel to the strip line. The picture on the left in part (b) shows the raw x-ray intensity image of the lamella. Next to it are the frames from a time-resolved normalized movie at 1.6 GHz excitation frequency arranged in a time series. The frames show dynamic changes in the normal magnetization component as gray scale contrast. The vertical wavefronts of the BV type waves can clearly be seen, as well as their horizontal propagation between the time frames (available also as animation M1 in the supplementary material for a better visualization). From such movies, the visual representation shown in the images in part (c) have been obtained, showing the color coded Fourier amplitude and phase at each pixel (cf. Sec. II). As expected for spin waves in a thin film, a transition from phase-front orientation normal to the external field (BV geometry) toward orientation parallel to the external field (DE geometry) can be observed when the frequency is raised, with intermediate phase-front orientations in between.[12] As is apparent in the first image (1.4 GHz) of the sequence, for the lowest frequencies, the spin waves were confined to the sample edges due to the locally reduced effective field because of demagnetization effects as previously described in the literature[58–60] and further discussed in the supplementary material (3) and Fig. S2. The region of confinement extended from the edges to about $0.5\,\mu$m into the sample. In the second image (1.6 GHz), which corresponds to the time series above, two coexisting BV waves of different wavelengths ($\lambda_1 = 1.9\,\mu$m and $\lambda_2 = 0.37\,\mu$m) are visible. Likewise, in the last two images (2.5 and 2.7 GHz, respectively), where the waves are fully in DE orientation, two DE modes of different wavelengths appear, coexisting at the same frequency (at $f = 2.7$ GHz: $\lambda_1 = 2.8\,\mu$m and $\lambda_2 = 0.53\,\mu$m). At intermediate frequencies of 2.0 GHz and 2.3 GHz, waves with diagonal phase fronts in between the two fundamental orientations can be observed.

In a second step, excitation was changed from continuous sine wave to short bursts [cf. Fig. 3(a)]. These bursts excited a broad spectrum of frequencies and, thus, a multitude of spin-wave modes simultaneously [one such normalized movie (M2) is attached as supplementary material M2]. The center frequency of $f = 2$ GHz was chosen corresponding to the previously identified modes and thereby to cover a rich spin-wave spectrum. The length of the burst was set to one sine period, or $\tau = 480$ ps, while the downtime to the next burst was set to 31 sine periods, or approximately $\tau' = 15$ ns. Single frequency components were isolated by a Fourier transform and, as previously, visualized in Fig. 3. The behavior is very similar to the continuous wave experiments shown in Fig. 2, especially for the direct comparison with the series in row (c) measured at the same field strength ($\mu_0 H_{ext} = 25$ mT). A transition from the BV to the DE propagation geometry at higher frequencies via diagonal intermediate orientations can be seen at all three magnetic bias field strengths. In agreement with theory,[4,8] the spin-wave spectra, and hence the transition point, shift toward higher frequencies for increasing external fields.

As the antenna was oriented for DE geometry excitation, its field is unlikely to be the primary source of the non-DE modes in the lamella. This point is reinforced by the observation that those waves do not originate in the antenna's vicinity but are rather excited at the lamella's edges, making the aforementioned edge demagnetization fields the probable cause for their existence. This mechanism, in which the localized edge field acts as a quasiantenna for spin-wave excitation, was originally suggested by Schlömann[61] and was supported by several experimental studies.[62–64] In particular for the BV geometry waves, the observed transition from edge confined modes to sample-wide BV modes hints at the edge fields as a source of the short-wavelength excitation. Here, the low k-value BV waves appear with outward propagating phase (negative group velocity) from both edges, while high k-value waves exhibit inward propagating phases. The aforementioned short-wavelength DE mode also appears to originate from the upper and lower sample edge rather than from the antenna region. This is presumably a consequence of the dynamically induced edge demagnetizing fields resulting from the antenna-emitted long DE-waves arriving at these edges.[64]

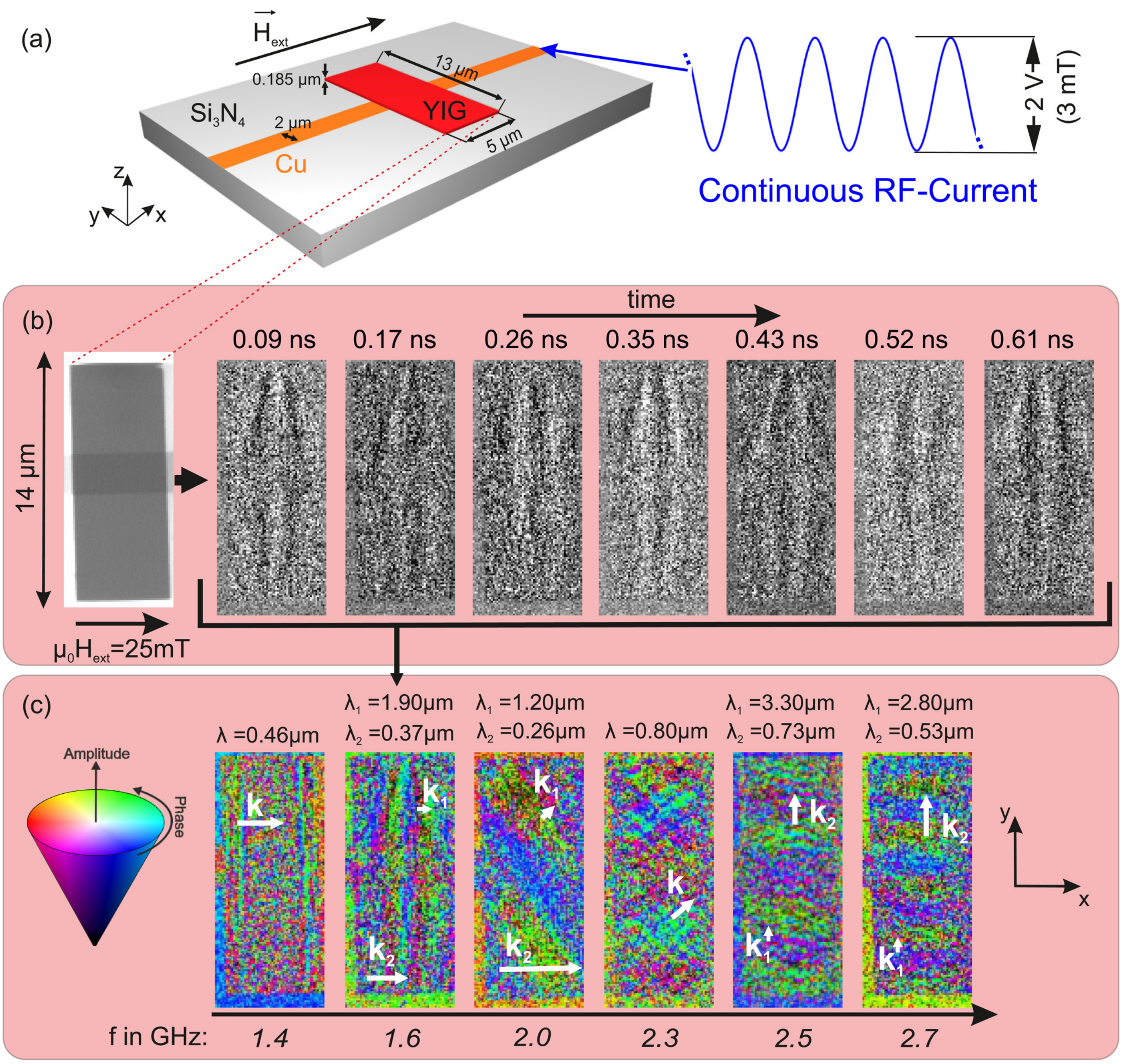

FIG. 2. (a) Schematics of the sample used for the experiments. Gray: silicon nitride membrane (Silson Ltd.). Red cuboid: YIG Lamella, dimensions: $13 \times 5 \times 0.185\,\mu m^3$. The magnetic bias field $\boldsymbol{H}_{ext}$ was oriented in the sample plane parallel to the copper strip line (x-direction). Red boxes: TR-STXM measurements of the sample at $\mu_0 H_{ext} = 25\,$mT and frequencies from 1.4 to 2.7 GHz. Left picture in (b) shows a raw x-ray image of the lamella (dark gray rectangle) and the strip line. The image series next to it displays the frames of a time-resolved movie at 1.6 GHz, showing the normalized (see Sec. II) out-of-plane magnetization in arbitrary units. The color images in (c) have been obtained from such movies by gaining the local Fourier amplitude and phase (cf. Sec. II) of each pixel's time-evolution and visualizing it in the HSV color space (color code on the lower left). Wave fronts visibly change from backward volume orientation, through diagonal intermediate states, to the Damon-Eshbach direction as the frequency increases. Wave vector directions are indicated in the images with the corresponding wavelengths λ stated above.

B. Analytical theory

To identify the specific spin waves that have been measured, their dispersion $f(k)$, where f is the frequency and $k = 2\pi/\lambda$ is the magnitude of the wavevector $\boldsymbol{k}$, was determined by a two-dimensional FFT (cf. Sec. II). The focus was put on the two fundamental wave orientations, namely, the BV geometry ($\theta = 0°$) and the DE geometry ($\theta = 90°$), with θ being the angle between $\boldsymbol{k}$ and the equilibrium magnetization. A quantitative analysis of the

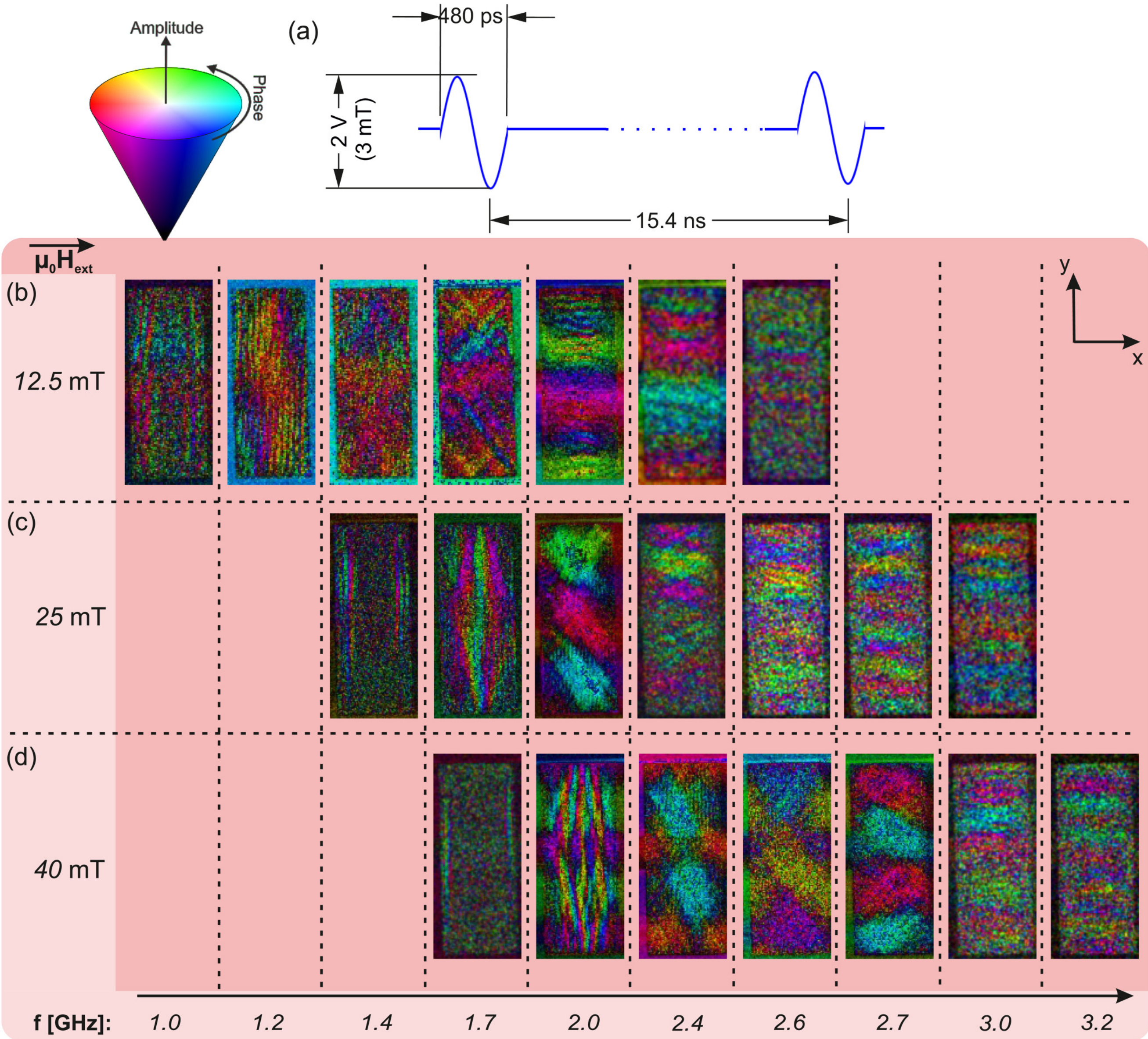

FIG. 3. (a): RF-burst signal used for the excitation of the sample (Duration: 480 ps, repetition time: 15.4 ns, voltage amplitude: 2V). Red box: Results of burst measurements analog to Fig. 2(c) at three different magnetic bias fields $\boldsymbol{H}_{ext}$ [(b): 12.5 mT, (c): 25 mT, (d): 40 mT]. Spin waves shift from the backward volume to the Damon-Eshbach propagation geometry as the frequency is raised, the transition point and general spectrum shifting to higher frequencies at greater field strength.

dispersion of the diagonal modes with intermediate angles ($0° < \theta < 90°$) was omitted in the scope of this work, yet in principle their dispersion can be analogously calculated using the theory discussed below [see Eq. (4)]. From a qualitative point of view, such diagonal waves are predicted to occur at frequencies in between those of the BV and DE geometries which is in agreement with our experimental observations. Proceeding with the analysis, pairs of f and k were accordingly sorted by their θ-values (0°, 90°) and compared to analytical models of basic spin wave modes in thin YIG films. A model for spin waves in a thin ferromagnetic layer can be found in the work of Kalinikos and Slavin,[12] taking the following approach.

An isotropic ferromagnetic film is considered that is laterally infinite and of finite thickness d along the z axis ($z \in [-d/2, d/2]$). The film is magnetized in-plane by a magnetic bias field. A plane spin wave with a nonuniform vector amplitude

$\boldsymbol{m}(z)$ is assumed to propagate in the film plane in the arbitrary ζ direction,

$$\boldsymbol{m}(z, \zeta, t) = \boldsymbol{m}(z) exp[i(\omega t - k\zeta)], \tag{1}$$

where t is time and $\omega = 2\pi f$. The amplitude $\boldsymbol{m}(z)$ is then expanded into an infinite series of complete orthogonal vector functions. For this, the eigenfunctions of the second-order exchange differential operator satisfying the appropriate exchange boundary conditions are chosen. For zero surface anisotropy (unpinned surface spins), which will be assumed from here on, this gives

$$\boldsymbol{m}(z) \propto \sum_n \boldsymbol{m}_n cos\left[\kappa_n\left(z + \frac{d}{2}\right)\right], \tag{2}$$

where $\kappa_n = n\pi/d$, $n \in \mathbb{N}_0$, represents a standing wave component perpendicular to the film plane. Using Eq. (2), the following infinite system of algebraic equations can be obtained from the well-known Landau-Lifshitz equation of motion,

$$-i\frac{\omega}{\omega_M}\boldsymbol{m}_n = \sum_{n'} \hat{W}_{nn'}\boldsymbol{m}_{n'}, \tag{3}$$

where $\omega_M = \gamma M_S$, γ is the gyromagnetic ratio [assumed 1.76×10^{11} rad/(sT) in calculations], and M_S is the saturation magnetization. This corresponds to Eq. (22) in the source paper,[12] where details on the square matrix $\hat{W}$ can also be found. The eigenvalues of this system give the frequency of the in-plane propagating spin-wave modes of the film. The mode order n here represents a standing spin-wave component along the film thickness given by κ_n. For $k = 0$, the mode coincides with the nth order PSSW. This results in the amplitude profile $m(z)$ having n nodes along the film thickness. If only the diagonal parts ($n = n'$) of $\hat{W}$ are considered, which means that interactions between modes of different orders are neglected, an approximate dispersion equation can be explicitly formulated,[12]

$$f_n(K) = \frac{\omega_H}{2\pi}\left\{\left(1 + \frac{M_S}{H}\, l_{ex}^2 K^2\right) \times \left(1 + \frac{M_S}{H}\, l_{ex}^2 K^2 + \frac{M_S}{H}\, F_{nn}\right)\right\}^{1/2} \tag{4}$$

with $K^2 = k^2 + \kappa_n^2$, $\omega_H = \gamma H$, the exchange length $l_{ex} = \sqrt{2A/(\mu_0 M_S^2)}$ and the element of the dipole-dipole matrix,

$$F_{nn} = 1 - P_{nn}cos^2\theta + P_{nn}(1 - P_{nn})\sin^2\theta \frac{M_S}{H + M_S\, l_{ex}^2 K^2}, \tag{5}$$

where H is the magnitude of the magnetic field, μ_0 is the vacuum permeability, A is the exchange constant, and θ is the angle between the magnetization and $\boldsymbol{k}$. For the fundamental zero-order mode (uniform thickness profile, no PSSW-component), $P_{00} = 1 - \frac{1-e^{-kd}}{kd}$ (see the Appendix of the original paper[12]). The zero-order equation gives the dispersions of the fundamental DE and BV modes at $\theta = 90°$ and $\theta = 0°$, respectively.[65]

C. Comparing theory and experimental data

In Fig. 4, the spin-wave dispersion relation, as deduced from the experimental data of both continuous wave and burst excitations for $\mu_0 H_{ext} = 25$ mT, is shown representatively. Analogous dispersion diagrams for the other two fields [Fig. 3(b) ($\mu_0 H_{ext} = 12.5$ mT) and (d) ($\mu_0 H_{ext} = 40$ mT)] can be found in the supplementary material. As Figs. 2 and 3 already suggested, it is not possible to distinguish between the dispersions measured for the two different excitation schemes, as the two data sets almost perfectly overlap. In a first step, the corresponding theoretical dispersion curves based on the approximate equation (4) were calculated (M_S given in Sec. II, $A = 0.36 \times 10^{-11}$ J/m[66]) and plotted in Fig. 4 as dashed lines. The $\theta = 0°$-waves fit very well with the calculated fundamental BV dispersion curve (dashed black line). The influence of the exchange interaction becomes clear by means of the curve changing to a positive slope beyond $k \approx 1 \times 10^7$ rad/m (compare to exchange free curves in Refs. 4 and 8). In the underlying Eq. (4), the exchange-related terms are quadratic in K. These terms are becoming larger than the terms related to the dipole-dipole interaction starting from the point where the spin wave dispersion has a minimum. Beyond this point, exchange is becoming dominant and determines the overall quadratic dispersion for sufficiently large values of K. It might be of note that this happens already at wavelengths more than an order of magnitude higher than the material's exchange length l_{ex}. The fact that the dispersion curve has a minimum explains the appearance of two coexisting BV-like waves shown in Fig. 2. These two waves originate from the dispersion regions with negative and positive group velocity at the left and right sides of the dispersion minimum. Thus, it appears that Eq. (4) is a valid approximation for BV waves in this sample, at least in the wavelength range covered here. There seems to be no significant hybridization with higher order BV modes and or influence of the confined sample geometry besides them originating from the lateral edges. The edge modes, shown by the green dots, come close to the BV dispersion with a downward frequency shift of about 200 MHz. In order to explain this difference through edge demagnetization effects, a reduction of the effective field to about 15 mT would be necessary. According to micromagnetic simulations of the lamella's demagnetizing field, this is a reasonable value at the edges, cf. supplementary material (3) and Fig. S2.

The $\theta = 90°$-waves, on the other hand, appear to belong to two separate dispersion branches that coexist in the area between $f = 2.5$ to 2.9 GHz. As mentioned earlier (cf. Fig. 2), two modes at $\theta = 90°$ can be seen simultaneously in the last images ($f \geq 2.5$ GHz), which already hints at this behavior. While the analytically approximated fundamental DE dispersion (dashed red line) fits the longer wavelength mode, the shorter wavelength one has to belong to a different spinwave mode featuring the same propagation direction. Obvious candidates for this are DE modes of higher orders. The dashed blue line in Fig. 4 represents the diagonal approximation for the first order thickness mode ($n = 1$) by Eq. (4). It is apparent that this approximation, i.e. neglecting hybridization between different mode orders, is insufficient to describe the DE first order thickness mode in this particular system.

Thus, in a second step, numerical calculations of the zero and first order DE dispersions have been carried out using the more

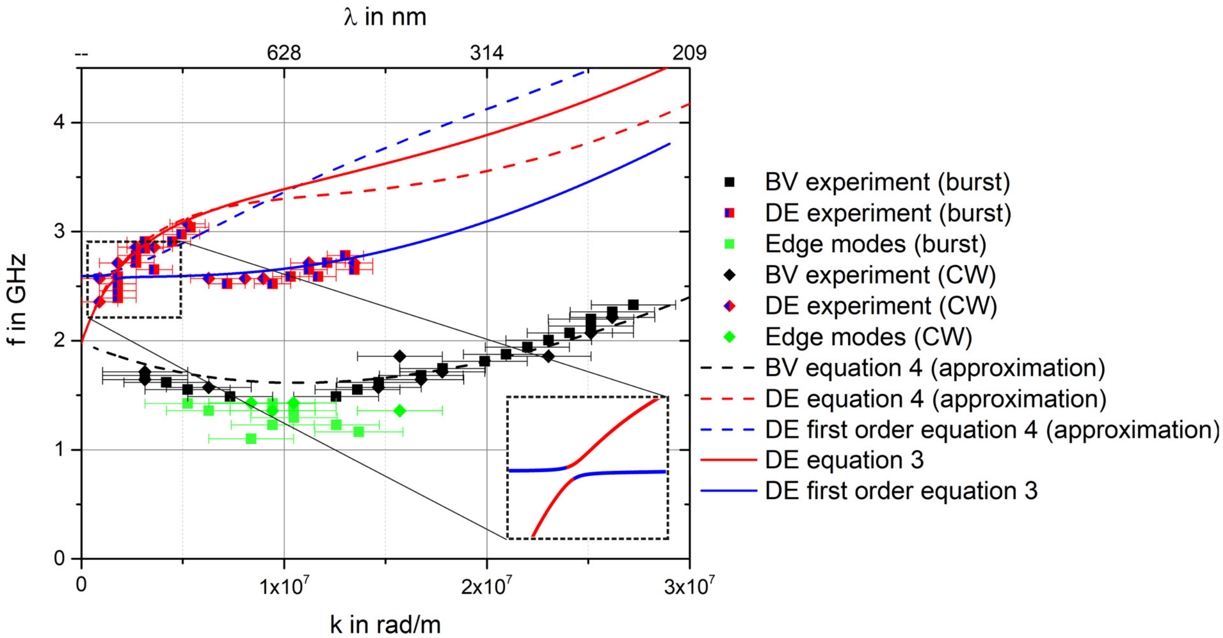

FIG. 4. Plot of experimental dispersion data at $\mu_0 H_{ext} = 25\,\mathrm{mT}$ for both continuous wave experiments (cf. Fig. 2) and the RF-burst experiment (cf. Fig. 3). Dots represent measured data sorted by propagation direction of the waves. Black and green dots show backward volume (BV) propagation ($\theta = 0°$) with the green dots marking those confined to the sample edges. The red-blue dots represent Damon-Eshbach(DE) propagation ($\theta = 90°$). Dashed lines show theoretical dispersion calculated using the approximate Eq. (4) (no hybridization). The red and blue lines show the zero and first order DE dispersions, while the black line stands for the BV mode. The solid lines represent DE dispersion based on numerical calculations according to Eq. (3), taking into account the hybridization of modes. The inset shows a magnification of the avoided crossing region of the two branches.

accurate equation system (3) and considering the nondiagonal terms $n \neq n'$ of the matrix. The results are shown as solid lines (red and blue) in Fig. 4 and they notably diverge from the dashed analytical curves, while they agree very well with the experimental data. This strongly suggests that the two modes indeed hybridize. A closer look at the modes' crossing point (inset in Fig. 4) supports this, as the presence of hybridization effects results in a band splitting. However, comparing the dashed and solid curves, it can be seen that the influence of the modes' mutual interaction reaches well beyond the crossing point. This agrees with observations made previously in 80 to 100 nm thick permalloy films.[43] Due to this, even the dispersion of the fundamental DE wave clearly diverges from the approximation of Eq. (4) below wavelengths of 600 nm. This stresses the importance of using the extended calculation when going below 1 μm wavelength.

Note that from an experimental point of view, the first order DE mode can only be observed by TR-STXM because hybridization effects are even more significant for the profile of the dynamic magnetization over the film thickness. A fully antisymmetric profile, as indicated in Fig. 1(e) for the $k = 0$ (ferromagnetic resonance) case, would render TR-STXM insensitive to the corresponding magnetization dynamics, because the signal it collects is integrated over the film thickness. However, mode hybridization causes the nodal line of the perpendicular dynamic magnetization component to shift away from its initially central position at higher frequencies, thereby providing a net contrast of dynamic magnetization given by the dominating fraction of perpendicular dynamic magnetization.[43]

Further note that confinement effects from the finite lateral size of the lamella are significant only for the occurrence of the edge-type modes discussed above as well as for a slight lateral variance of the dispersion, stemming from a lateral variation of the local demagnetization field, as can be seen in Figs. 3(b) and 5 (upper panel, 1.6 GHz) (cf. also supplementary material (3) and Fig. S2). Although laterally standing modes were partially observed in the experiments in combination with dominating propagating waves (supplementary material, movie M1), they did not have a significant influence on the corresponding spin-wave dispersion. This is mainly for two reasons: (i) the inhomogenous line-broadening of the YIG thin film of $\Delta H_0 = 0.13$ mT limits the spin-wave lifetime to about 100 ns, and the corresponding BV propagation lengths to the order of 10 μm, respectively. Thereby, standing wave patterns are substantially reduced in amplitude. (ii) A possible frequency discretization of propagating waves[58,67] and hybridization of waves of higher lateral order turns out to be negligible in our experimental scales. As further discussed in the supplementary material (4), Fig. S3, at $k = 5\,\mathrm{rad}/\mu\mathrm{m}$, such a discretization would be of the order of 25 MHz and reducing to higher k-values, which is below the experimental grid of investigated frequencies.

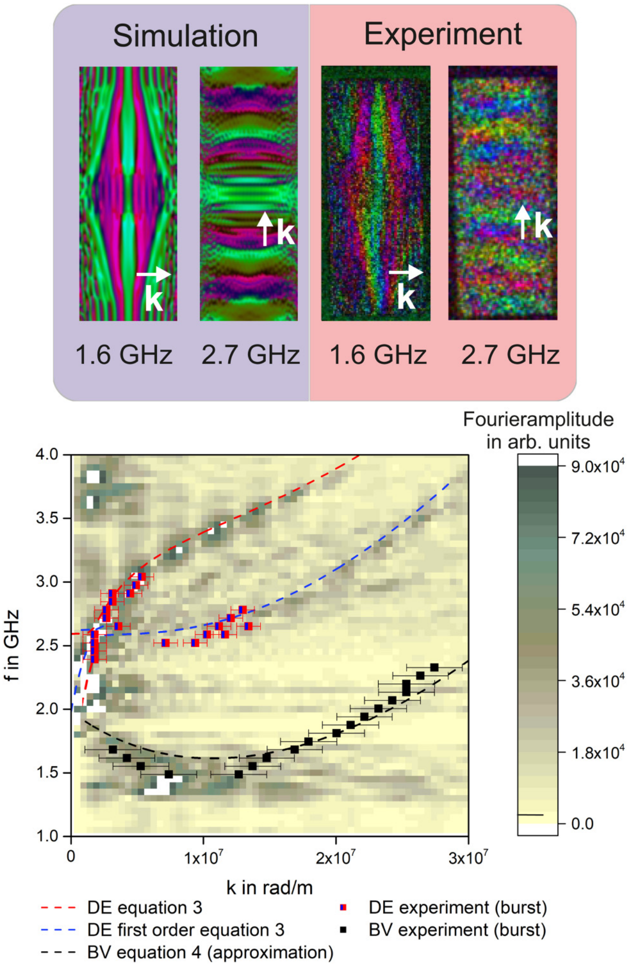

FIG. 5. Upper part: Direct comparison of Fourier images of the experiment and the micromagnetic simulation at $\mu_0 H = 25$ mT. Lower part: Heatmap of the spatial Fourier transform of the simulation for the two main directions $\theta = 0°$ and $\theta = 90°$ with the corresponding experimental data (dots) and theoretical dispersion relations (dashed lines) for the Damon-Eshbach modes of order zero and one based on Eq. (3), as well as for the backward volume mode based on Eq. (4).

D. Micromagnetic simulation

Finally, a micromagnetic simulation was carried out using the "MuMax 3" software developed by Vansteenkiste *et al.*[68] For the simulation, the same material parameters as for the dispersion calculations were used. The discretization size of the simulations was set to 10 nm in all three dimensions, which is sufficiently below the exchange length of YIG (approximately 16.7 nm). An external field of $\mu_0 H = 25$ mT was considered together with an RF-burst excitation similar to the experimental one with a field amplitude of 3 mT. Figure 5 shows direct comparisons of Fourier images from the simulation and experiments at two different frequencies. It can be seen that the simulation reproduces the experimental dynamics qualitatively. One notable aspect confirmed by the simulation is that the phase fronts of the BV waves at 1.6 GHz vary along the lamella's y axis (cf. Fig. 5, upper panel), which is a consequence of the local effective magnetic field distribution in this direction. Note that this effect scales with the field dependence of a particular spin-wave frequency. Quantitative results for the dispersion along the main directions $\theta = 0°$ and $\theta = 90°$ are depicted in the lower part of Fig. 5 and show reasonable agreement with the physical measurements (dots) and theory accounting for hybridization (dashed lines). This gives a reason to assume that the simulation is a good representation of the experiment and that the simulation results beyond the experimentally covered region represent a viable extrapolation. The agreement of simulation and theory in such advanced regions further supports the theoretical approach taken.

The simulation also highlights another important point. As Fig. 5 shows, the dispersion curves in theory and simulation continue beyond the experimentally observed data range. This is especially apparent for the DE-waves, which stay well below the wavenumbers measured in the BV geometry, that themselves reach a limit at $k \approx 3 \times 10^7$ rad/m ($\lambda \approx 200$ nm). Physically, for every antennalike spin-wave source, there is a sharply diminishing efficiency of excitation for wavelengths below the source's width. This limits the wavevectors that can be excited by the source at a given energy input. Since the BV waves are likely excited by the demagnetization fields on the lateral edges, which featured narrow peaks of less than 0.5 μm width [cf. supplementary material (3) and Fig. S2], the limit for them is lower than for the zero-order DE-waves, which are excited by the 2 μm wide copper antenna, hence, the occurrence of much shorter waves in the BV geometry.

IV. CONCLUSIONS

In summary, spin waves of wavelengths down to 200 nm have been directly imaged in YIG using TR-STXM. For this, a nearly freestanding lamella was fabricated from a YIG film by focused ion beam preparation. Spin-wave modes of various directions in the sample plane have been recorded as a function of frequency and external magnetic field. TR-STXM enabled the simultaneous determination of their spatial properties, like wavefront shape, propagation direction or confinement to certain regions (e.g., the edge), and of the waves' time domain features. Dynamics were excited by continuous single frequency RF-fields as well as by broadband RF-bursts. The observed BV waves agree very well with a simple diagonal approximation of the analytical expression for the dispersion relation.[12] This approach still held reasonably for the zero-order DE mode up to $k \approx 6 \times 10^6$ rad/m. However, a second DE dispersion branch was observed, leading to the coexistence of two DE modes with strongly different wavelengths in the frequency range between 2.5 and 2.9 GHz. The diagonal approximation does not correctly describe the second mode, neither as DE zero order nor as its first higher order thickness mode. A more rigorous numerical calculation based on the full set of equations[12] was necessary and provided an excellent match with the experimental findings. It can be concluded that hybridization between different mode orders plays a major role in this system for the formation of spin waves propagating in the DE geometry. Micromagnetic simulations have been done and fit well with the experimental data and the calculated dispersions, indicating their potential to predict the observed magnonic scenario in the system studied. While all analytic calculations assumed a laterally infinite film, it appears that the measured wavelengths were sufficiently small compared to the dimensions of the sample to still warrant this assumption.

The presented work demonstrates that TR-STXM is a powerful and versatile tool for high resolution imaging of magnetization dynamics in real space and time domain. It clearly demonstrates its applicability to YIG thin films, making these accessible to space and time-resolved spin-wave studies beyond optical resolution limits. We have furthermore shown a way to isolate high-quality YIG films from their growth-required GGG substrates, a prerequisite to avoid parasitic electron paramagnetic resonance losses at low temperatures for quantum computing applications. Our study opens up a pathway to directly image nanoscaled spin dynamics in YIG and other single-crystalline materials, and it will have an important impact for fundamental magnonic research and applications in nanodevices.

SUPPLEMENTARY MATERIAL

See the supplementary material for the original video files of a selection of the experimental measurements shown in Figs. 2 and 3 with some additional information on the measurement parameters. It also contains the dispersion diagrams for the experiments at $\mu_0 H_{ext} = 12.5$ and 40 mT analogous to Fig. 4. Furthermore, calculations of the internal magnetic field of the lamella along the x-direction, supposedly responsible for the Schlömann-like excitation of the BV modes, are presented to support this conclusion. Finally, the effects of the lateral confinement on the spin-wave dispersion are discussed in more detail and calculated dispersion curves are presented that show these effects to be minor.

ACKNOWLEDGMENTS

We would like to thank Doris Meertens (formerly FZ Jülich) for the FIB preparation of the YIG lamella as well as Oleksii Surzhenko (Innovent Jena) for the ferromagnetic resonance measurements. Michael Bechtel (MPI-IS) is gratefully acknowledged for support during beamtimes. We thank HZB for the allocation of synchrotron radiation beamtime. J.B. is supported from the European Union's Horizon 2020 Research and Innovation Programme under the Marie Skłodowska-Curie Grant Agreement No. 66566. C.D. acknowledges financial support by the Deutsche Forschungsgemeinschaft (DFG) under contract No. DU 1427/2-1. A.N.S. was supported by Grant Nos. EFMA-1641989 and ECCS-1708982 from the National Science Foundation (NSF) of the U.S.A., and by the Defense Advanced Research Projects Agency (DARPA) M3IC Grant under Contract No. W911-17-C-0031.

REFERENCES

[1]S. O. Demokritov, V. E. Demidov, O. Dzyapko, G. A. Melkov, A. A. Serga, B. Hillebrands, and A. N. Slavin, "Bose–Einstein condensation of quasi-equilibrium magnons at room temperature under pumping," Nature **443**, 430 (2006).
[2]D. A. Bozhko, A. A. Serga, P. Clausen, V. I. Vasyuchka, F. Heussner, G. A. Melkov, A. Pomyalov, V. S. L'vov, and B. Hillebrands, "Supercurrent in a room-temperature Bose–Einstein magnon condensate," Nat. Phys. **12**, 1057 (2016).
[3]A. Roldán-Molina, A. S. Nunez, and R. Duine, "Magnonic black holes," Phys. Rev. Lett. **118**, 061301 (2017).
[4]A. A. Serga, A. V. Chumak, and B. Hillebrands, "YIG magnonics," J. Phys. D Appl. Phys. **43**, 264002 (2010).
[5]A. V. Chumak, V. I. Vasyuchka, A. A. Serga, and B. Hillebrands, "Magnon spintronics," Nat. Phys. **11**, 453 (2015).
[6]S. Kosen, A. F. v. Loo, D. A. Bozhko, L. Mihalceanu, and A. D. Karenowska, "Microwave magnon damping in YIG films at millikelvin temperatures," APL Matererials **7**(10), 101120 (2019).
[7]L. Mihalceanu, V. I. Vasyuchka, D. A. Bozhko, T. Langner, A. Y. Nechiporuk, V. F. Romanyuk, B. Hillebrands, and A. A. Serga, "Temperature-dependent relaxation of dipole-exchange magnons in yttrium iron garnet films," Phys. Rev. B **97**, 214405 (2018).
[8]D. D. Stancil and A. Prabhakar, *Spin Waves, Theory and Applications*, 1st ed., Vol. 348 (Springer US, 2009), pp. XII.
[9]R. W. Damon and H. v. d. Vaart, "Dispersion of spin waves and magnetoelastic waves in YIG," Proc. IEEE **53**, 348–354 (1965).
[10]H. J. J. Liu, G. A. Riley, and K. S. Buchanan, "Directly excited backward volume spin waves in permalloy microstrips," IEEE Magn. Lett. **6**, 1–4 (2015).
[11]S. Klingler, P. Pirro, T. Brächer, B. Leven, B. Hillebrands, and A. V. Chumak, "Spin-wave logic devices based on isotropic forward volume magnetostatic waves," Appl. Phys. Lett. **106**, 212406 (2015).
[12]B. A. Kalinikos and A. N. Slavin, "Theory of dipole-exchange spin wave spectrum for ferromagnetic films with mixed exchange boundary conditions," J. Phys. C Solid State Phys. **19**, 7013 (1986).
[13]D. A. Bozhko, P. Clausen, G. A. Melkov, V. S. L'vov, A. Pomyalov, V. I. Vasyuchka, A. V. Chumak, B. Hillebrands, and A. A. Serga, "Bottleneck accumulation of hybrid magnetoelastic bosons," Phys. Rev. Lett. **118**, 237201 (2017).
[14]A. J. E. Kreil, D. A. Bozhko, H. Y. Musiienko-Shmarova, V. I. Vasyuchka, V. S. L'vov, A. Pomyalov, B. Hillebrands, and A. A. Serga, "From kinetic instability to Bose-Einstein condensation and magnon supercurrents," Phys. Rev. Lett. **121**, 077203 (2018).
[15]A. A. Serga, V. S. Tiberkevich, C. W. Sandweg, V. I. Vasyuchka, D. A. Bozhko, A. V. Chumak, T. Neumann, B. Obry, G. A. Melkov, A. N. Slavin, and B. Hillebrands, "Bose–Einstein condensation in an ultra-hot gas of pumped magnons," Nat. Commun. **5**, 3452 (2014).
[16]M. Kaack, S. Jun, S. A. Nikitov, and J. Pelzl, "Magnetostatic spin wave modes excitation in yttrium iron garnet film under various temperatures," J. Magn. Magn. Mater. **204**, 90–100 (1999).
[17]J. S. Baek, S. Y. Ha, W. Y. Lim, and S. H. Lee, "Magnetostatic wave study of YIG films grown by the LPE method," Phys. Status Solidi (a) **201**, 1806–1809 (2004).
[18]T. Fischer, M. Kewenig, D. A. Bozhko, A. A. Serga, I. I. Syvorotka, F. Ciubotaru, C. Adelmann, B. Hillebrands, and A. V. Chumak, "Experimental prototype of a spin-wave majority gate," Appl. Phys. Lett. **110**, 152401 (2017).
[19]H. T. Nembach, J. M. Shaw, C. T. Boone, and T. J. Silva, "Mode- and size-dependent Landau-Lifshitz damping in magnetic nanostructures: Evidence for nonlocal damping," Phys. Rev. Lett. **110**, 117201 (2013).
[20]R. Adur, C. Du, H. Wang, S. A. Manuilov, V. P. Bhallamudi, C. Zhang, D. V. Pelekhov, F. Yang, and P. C. Hammel, "Damping of confined modes in a ferromagnetic thin insulating film: Angular momentum transfer across a nanoscale field-defined interface," Phys. Rev. Lett. **113**, 176601 (2014).
[21]A. Talalaevskij, M. Decker, J. Stigloher, A. Mitra, H. S. Körner, O. Cespedes, C. H. Back, and B. J. Hickey, "Magnetic properties of spin waves in thin yttrium iron garnet films," Phys. Rev. B **95**, 064409 (2017).
[22]J. P. Park, P. Eames, D. M. Engebretson, J. Berezovsky, and P. A. Crowell, "Spatially resolved dynamics of localized spin-wave modes in ferromagnetic wires," Phys. Rev. Lett. **89**, 277201 (2002).
[23]M. Collet, O. Gladii, M. Evelt, V. Bessonov, L. Soumah, P. Bortolotti, S. O. Demokritov, Y. Henry, V. Cros, M. Bailleul, V. E. Demidov, and A. Anane,

"Spin-wave propagation in ultra-thin YIG based waveguides," Appl. Phys. Lett. **110**, 092408 (2017).
[24]T. Sebastian, K. Schultheiss, B. Obry, B. Hillebrands, and H. Schultheiss, "Micro-focused Brillouin light scattering: Imaging spin waves at the nanoscale," Front. Phys. **3**, 35 (2015).
[25]M. Agrawal, V. I. Vasyuchka, A. A. Serga, A. D. Karenowska, G. A. Melkov, and B. Hillebrands, "Direct measurement of magnon temperature: New insight into magnon-phonon coupling in magnetic insulators," Phys. Rev. Lett. **111**, 107204 (2013).
[26]J. Jersch, V. E. Demidov, H. Fuchs, K. Rott, P. Krzysteczko, J. Münchenberger, G. Reiss, and S. O. Demokritov, "Mapping of localized spin-wave excitations by near-field Brillouin light scattering," Appl. Phys. Lett. **97**, 152502 (2010).
[27]P. S. Keatley, T. H. J. Loughran, E. Hendry, W. L. Barnes, R. J. Hicken, J. R. Childress, and J. A. Katine, "A platform for time-resolved scanning Kerr microscopy in the near-field," Rev. Sci. Instrum. **88**, 123708 (2017).
[28]H. Yu, O. d' Allivy Kelly, V. Cros, R. Bernard, P. Bortolotti, A. Anane, F. Brandl, F. Heimbach, and D. Grundler, "Approaching soft x-ray wavelengths in nanomagnet-based microwave technology," Nat. Commun. **7**, 11255 (2016).
[29]M. Bailleul, D. Olligs, and C. Fermon, "Propagating spin wave spectroscopy in a permalloy film: A quantitative analysis," Appl. Phys. Lett. **83**, 972–974 (2003).
[30]G. de Loubens, V. V. Naletov, O. Klein, J. B. Youssef, F. Boust, and N. Vukadinovic, "Magnetic resonance studies of the fundamental spin-wave modes in individual submicron Cu/NiFe/Cu perpendicularly magnetized disks," Phys. Rev. Lett. **98**, 127601 (2007).
[31]B. Van Waeyenberge, A. Puzic, H. Stoll, K. W. Chou, T. Tyliszczak, R. Hertel, M. Fähnle, H. Brückl, K. Rott, G. Reiss, I. Neudecker, D. Weiss, C. H. Back, and G. Schütz, "Magnetic vortex core reversal by excitation with short bursts of an alternating field," Nature **444**, 461 (2006).
[32]Y. Acremann, J. P. Strachan, V. Chembrolu, S. D. Andrews, T. Tyliszczak, J. A. Katine, M. J. Carey, B. M. Clemens, H. C. Siegmann, and J. Stöhr, "Time-resolved imaging of spin transfer switching: Beyond the macrospin concept," Phys. Rev. Lett. **96**, 217202 (2006).
[33]Y. Acremann, V. Chembrolu, J. P. Strachan, T. Tyliszczak, and J. Stöhr, "Software defined photon counting system for time resolved X-ray experiments," Rev. Sci. Instrum. **78**, 014702 (2007).
[34]M. Weigand, B. Van Waeyenberge, A. Vansteenkiste, M. Curcic, V. Sackmann, H. Stoll, T. Tyliszczak, K. Kaznatcheev, D. Bertwistle, G. Woltersdorf, C. H. Back, and G. Schütz, "Vortex core switching by coherent excitation with single in-plane magnetic field pulses," Phys. Rev. Lett. **102**, 077201 (2009).
[35]A. Puzic, T. Korhonen, B. Kalantari, J. Raabe, C. Quitmann, P. Jüllig, L. Bommer, D. Goll, G. Schütz, S. Wintz, T. Strache, M. Körner, D. Marko, C. Bunce, and J. Fassbender, "Photon counting system for time-resolved experiments in multibunch mode," Synchrotron. Radiat. News. **23**, 26 (2010).
[36]C. Cheng and W. E. Bailey, "Sub-micron mapping of GHz magnetic susceptibility using scanning transmission x-ray microscopy," Appl. Phys. Lett. **101**, 182407 (2012).
[37]D. Nolle, M. Weigand, P. Audehm, E. Goering, U. Wiesemann, C. Wolter, E. Nolle, and G. Schütz, "Note: Unique characterization possibilities in the ultra high vacuum scanning transmission x-ray microscope (UHV-STXM) "maxymus" using a rotatable permanent magnetic field up to 0.22 T," Rev. Sci. Instrum. **83**, 046112 (2012).
[38]M. Noske, A. Gangwar, H. Stoll, M. Kammerer, M. Sproll, G. Dieterle, M. Weigand, M. Fähnle, G. Woltersdorf, C. H. Back, and G. Schütz, "Unidirectional sub-100-ps magnetic vortex core reversal," Phys. Rev. B **90**, 104415 (2014).
[39]P. Wohlhüter, M. T. Bryan, P. Warnicke, S. Gliga, S. E. Stevenson, G. Heldt, L. Saharan, A. K. Suszka, C. Moutafis, R. V. Chopdekar, J. Raabe, T. Thomson, G. Hrkac, and L. J. Heyderman, "Nanoscale switch for vortex polarization mediated by Bloch core formation in magnetic hybrid systems," Nat. Commun. **6**, 7836 (2015).
[40]S. Bonetti, R. Kukreja, Z. Chen, F. Macià, J. M. Hernàndez, A. Eklund, D. Backes, J. Frisch, J. Katine, G. Malm, S. Urazhdin, A. D. Kent, J. Stöhr, H. Ohldag, and H. A. Dürr, "Direct observation and imaging of a spin-wave soliton with p-like symmetry," Nat. Commun. **6**, 8889 (2015).
[41]S. Bonetti, R. Kukreja, Z. Chen, D. Spoddig, K. Ollefs, C. Schöppner, R. Meckenstock, A. Ney, J. Pinto, R. Houanche, J. Frisch, J. Stöhr, H. A. Dürr, and H. Ohldag, "Microwave soft x-ray microscopy for nanoscale magnetization dynamics in the 5-10 GHz frequency range," Rev. Sci. Instrum. **86**, 093703 (2015).
[42]H. Stoll, M. Noske, M. Weigand, K. Richter, B. Krüger, R. M. Reeve, M. Hänze, C. F. Adolff, F.-U. Stein, G. Meier, M. Kläui, and G. Schütz, "Imaging spin dynamics on the nanoscale using x-ray microscopy," Front. Phys. **3**, 26 (2015).
[43]G. Dieterle, J. Förster, H. Stoll, A. S. Semisalova, S. Finizio, A. Gangwar, M. Weigand, M. Noske, M. Fähnle, I. Bykova, J. Gräfe, D. A. Bozhko, H. Y. Musiienko-Shmarova, V. Tiberkevich, A. N. Slavin, C. H. Back, J. Raabe, G. Schütz, and S. Wintz, "Coherent excitation of heterosymmetric spin waves with ultrashort wavelengths," Phys. Rev. Lett. **122**, 117202 (2019).
[44]S. Wintz, V. Tiberkevich, M. Weigand, J. Raabe, J. Lindner, A. Erbe, A. Slavin, and J. Fassbender, "Magnetic vortex cores as tunable spin-wave emitters," Nat. Nanotechnol. **11**, 948 (2016).
[45]J. Gräfe, M. Decker, K. Keskinbora, M. Noske, P. Gawronski, H. Stoll, C. Back, E. Goering, and G. Schütz, "X-ray microscopy of spin wave focusing using a Fresnel zone plate," e-print arXiv:1707.03664 [cond-mat.mes-hall] (2017).
[46]M. Kammerer, M. Weigand, M. Curcic, M. Noske, M. Sproll, A. Vansteenkiste, B. Van Waeyenberge, H. Stoll, G. Woltersdorf, C. H. Back, and G. Schuetz, "Magnetic vortex core reversal by excitation of spin waves," Nat. Commun. **2**, 279 (2011).
[47]F. Groß, N. Träger, J. Förster, M. Weigand, G. Schütz, and J. Gräfe, "Nanoscale detection of spin wave deflection angles in permalloy," Appl. Phys. Lett. **114**, 012406 (2019).
[48]J. Simmendinger, S. Ruoss, C. Stahl, M. Weigand, J. Gräfe, G. Schütz, and J. Albrecht, "Transmission x-ray microscopy at low temperatures: Irregular supercurrent flow at small length scales," Phys. Rev. B **97**, 134515 (2018).
[49]M. Fohler, S. Frömmel, M. Schneider, B. Pfau, C. M. Günther, M. Hennecke, E. Guehrs, L. Shemilt, D. Mishra, D. Berger, S. Selve, D. Mitin, M. Albrecht, and S. Eisebitt, "A general approach to obtain soft x-ray transparency for thin films grown on bulk substrates," Rev. Sci. Instrum. **88**, 103701 (2017).
[50]C. Dubs, O. Surzhenko, R. Linke, A. Danilewsky, U. Brückner, and J. Dellith, "Sub-micrometer yttrium iron garnet LPE films with low ferromagnetic resonance losses," J. Phys. D Appl. Phys. **50**, 204005 (2017).
[51]P. Pirro, T. Brächer, A. V. Chumak, B. Lägel, C. Dubs, O. Surzhenko, P. Görnert, B. Leven, and B. Hillebrands, "Spin-wave excitation and propagation in microstructured waveguides of yttrium iron garnet/Pt bilayers," Appl. Phys. Lett. **104**, 012402 (2014).
[52]A. Krysztofik, L. E. Coy, P. Kuświk, K. Załeęski, H. Głowiński, and J. Dubowik, "Ultra-low damping in lift-off structured yttrium iron garnet thin films," Appl. Phys. Lett. **111**, 192404 (2017).
[53]M. Kruth, D. Meertens, and K. Tillmann, Ernst Ruska-Centre for Microscopy and Spectroscopy with Electrons (ER-C), "Fei Helios Nanolab 460F1 FIB-SEM," J. Large-Scale Res. Facilities **2**, A42 (2016).
[54]G. Schütz, W. Wagner, W. Wilhelm, P. Kienle, R. Zeller, R. Frahm, and G. Materlik, "Absorption of circularly polarized X rays in iron," Phys. Rev. Lett. **58**, 737–740 (1987).
[55]B. B. Krichevtsov, S. V. Gastev, S. M. Suturin, V. V. Fedorov, A. M. Korovin, V. E. Bursian, A. G. Banshchikov, M. P. Volkov, M. Tabuchi, and N. S. Sokolov, "Magnetization reversal in YIG/GGG(111) nanoheterostructures grown by laser molecular beam epitaxy," Sci. Technol. Adv. Mater. **18**, 351–363 (2017).
[56]T. E. Oliphant, "Python for scientific computing," Comput. Sci. Eng. **9**, 10–20 (2007).
[57]J. D. Hunter, "Matplotlib: A 2d graphics environment," Comput. Sci. Eng. **9**, 90–95 (2007).
[58]J. Jorzick, S. O. Demokritov, B. Hillebrands, M. Bailleul, C. Fermon, K. Y. Guslienko, A. N. Slavin, D. V. Berkov, and N. L. Gorn, "Spin wave wells in nonellipsoidal micrometer size magnetic elements," Phys. Rev. Lett. **88**, 047204 (2002).

[59]C. Bayer, S. O. Demokritov, B. Hillebrands, and A. N. Slavin, "Spin-wave wells with multiple states created in small magnetic elements," Appl. Phys. Lett. **82**, 607–609 (2003).
[60]H. Puszkarski, M. Krawczyk, and J. C. S. Lévy, "Localization properties of pure magnetostatic modes in a cubic nanograin," Phys. Rev. B **71**, 014421 (2005).
[61]E. Schlömann, "Generation of spin waves in nonuniform magnetic fields. I. Conversion of electromagnetic power into spin-wave power and vice versa," J. Appl. Phys. **35**, 159–166 (1964).
[62]C. S. Davies, A. V. Sadovnikov, S. V. Grishin, Y. P. Sharaevskii, S. A. Nikitov, and V. V. Kruglyak, "Generation of propagating spin waves from regions of increased dynamic demagnetising field near magnetic antidots," Appl. Phys. Lett. **107**, 162401 (2015).
[63]C. S. Davies and V. V. Kruglyak, "Generation of propagating spin waves from edges of magnetic nanostructures pumped by uniform microwave magnetic field," IEEE. Trans. Magn. **52**, 1–4 (2016).
[64]C. S. Davies, V. D. Poimanov, and V. V. Kruglyak, "Mapping the magnonic landscape in patterned magnetic structures," Phys. Rev. B **96**, 094430 (2017).
[65]Note that, in the original Damon-Eshbach theory, a nonuniform thickness profile is considered, while the influence of exchange is neglected.[9]
[66]S. Klingler, A. V. Chumak, T. Mewes, B. Khodadadi, C. Mewes, C. Dubs, O. Surzhenko, B. Hillebrands, and A. Conca, "Measurements of the exchange stiffness of YIG films using broadband ferromagnetic resonance techniques," J. Phys. D Appl. Phys. **48**, 015001 (2015).
[67]J. Jorzick, S. O. Demokritov, C. Mathieu, B. Hillebrands, B. Bartenlian, C. Chappert, F. Rousseaux, and A. N. Slavin, "Brillouin light scattering from quantized spin waves in micron-size magnetic wires," Phys. Rev. B **60**, 15194–15200 (1999).
[68]A. Vansteenkiste, J. Leliaert, M. Dvornik, M. Helsen, F. Garcia-Sanchez, and B. V. Waeyenberge, "The design and verification of MuMax3," AIP Adv. **4**, 107133 (2014).